Journal of Theoretical and Applied Physics
a SpringerOpen Journal

RESEARCH Open Access

Analysis of discharge parameters and optimization study of coaxial DBDs for efficient excimer light sources

Udit Narayan Pal*, Pooja Gulati, Niraj Kumar, Mahesh Kumar, Vishnu Srivastava and Ram Prakash

Abstract

In this work, a xenon-filled quartz coaxial dielectric barrier discharge (DBD) tube (ID 6 mm, OD 12 mm) at 400-mbar pressure has been studied at different operating conditions. High-frequency sinusoidal and unipolar pulse-like voltages are applied at the discharge electrodes for the generation of micro-discharge plasma. Visual images of the discharge and the electrical waveform confirm the diffused-type discharge. The mechanism that is involved in the ignition, development and extinction of DBDs is quantitatively explained by dynamic processes in the discharge. An equivalent electrical model representing the DBD phenomenon has also been used to validate the characteristic discharge parameters. The relative intensity analysis of the Xe continuum peak at wavelength 172 nm in the optical emission spectra of the vacuum ultraviolet region has been carried out for different operating conditions. Approximately three times increment in the radiation is observed in pulse excitation over sinusoidal excitation. It infers that the pulsed excitation of DBD sources is advantageous for excimer light sources.

Keywords: Non-thermal plasma and non-equilibrium plasma, Dielectric barrier discharge (DBD), Micro-discharges, Diffused discharge, Equivalent electrical circuit

PACS: 52.80.Hc, 52.38.Hb, 52.70.Kz, 52.50.Dg, 52.80.Pi

Background

The dielectric barrier discharge (DBD) was originally proposed by Siemens in 1857 for 'ozonizing air', which is another way of generating non-local thermodynamical equilibrium plasmas even at atmospheric pressure [1,2]. For over a century, DBDs have been used for a number of industrial applications starting from ozone generation, surface modification, to flat plasma display panels [3,4]. Efficient excimer formation in DBDs is technically very important for use in high-power ultraviolet lamps. Excimer lamps are mercury-free systems and eco-friendly, and therefore, they are a boom for the lighting industry. In addition, DBDs enable various emerging novel applications in biology and the medical field [5-7].

Dielectric barrier-based discharges are traditionally driven by sinusoidal wave voltages with magnitudes in the kilovolt range and frequencies in the kilohertz range. To improve the energy transfer efficiency, voltage pulses with sub-microsecond rise and fall times have been proposed by several investigators [8,9]. Generally, two discharges are ignited per pulse: one at the rising edge and the second discharge at the falling edge of the voltage pulse [10]. Here, we performed the experiment with the unipolar pulse and sinusoidal applied waveforms for a xenon-filled coaxial DBD tube.

For electrical diagnostics of the discharge, a temporally dynamic model for diffuse DBDs is developed [11]. From this model, the calculations of internal electrical quantities in the discharge gap from measured external electrical quantities have been carried out. The experimentally measured total current (i.e. sum of the capacitive displacement current and the conduction current) is used to estimate the discharge current. The dynamic nature of voltages across the dielectric, memory voltage, gas gap voltage and charge accumulation of DBD are calculated from this model and correlated to the current measurements.

* Correspondence: paludit@gmail.com
Plasma Devices Group, Microwave Tubes Division, Council of Scientific and Industrial Research-Central Electronics Engineering Research Institute (CSIR-CEERI), Pilani 333031, India

Finally, the different components of the power (stored and dissipated) and relative intensities are calculated at various operating conditions. The relative intensity analysis of the Xe spectral line from the observed emission spectra has also been carried out, and around three times more vacuum ultraviolet (VUV) radiations of peak wavelength at 172 nm are observed in the case of pulse excitation compared to that of sinusoidal excitation.

Methods

DBD cell design

Figure 1a depicts the schematic of the coaxial DBD lamp consisting of two coaxially fused quartz tubes separated by a gas gap. Figure 1b shows the picture of a coaxial DBD cell filled with xenon (r_1 = 3 mm, r_2 = 5 mm). The outer surface of the quartz tube is wrapped by a copper wire mesh (mesh size 900 in.$^{-2}$, wire size 0.15 mm) electrode, and the inner electrode of Cusil foil (72% Ag and 28% Cu) has been inserted into the coaxial tube in close proximity to the inner wall. A high-voltage waveform is applied on the inner electrode, and on the other hand, the outer mesh electrode is grounded. The gas gap is kept 1 mm for the xenon-filled DBD. The total length of the xenon DBD cell is 90 mm, while the outer mesh and the inner foil electrode wrap 60 mm of the tube.

Experimental set-up

Figure 2 shows the schematic view of the experimental set-up. For plasma generation in DBDs, both bipolar sine wave and unipolar pulses are applied between the two electrodes. A high-voltage unipolar pulse power supply up to a −6-kV peak voltage along with different frequency ranges up to 30 kHz (GROWCONTROLS HV Pulse Power Supply, GC503HVPPS, Hyderabad, India) and also a high-voltage sinusoidal supply (Huettinger HF Generator TIG 10/100 PSC, Freiburg, Germany) up to a 2.4-kV peak voltage with frequencies between 20 and 100 kHz have been applied to the discharge electrodes for the generation of micro-discharge plasma. The DBD tube has been mounted on a vacuum pumping system and evacuated up to a base pressure of approximately 5×10^{-6} mbar. At room temperature, xenon gas of 99.99% purity (Matheson Gases, Albuquerque, NM, USA) has been filled in the DBD tube to operate it at different working pressures. A high-voltage signal is applied to the inner electrode, while the outer mesh electrode is grounded. The wire mesh electrode allows the radiation to come out of the tube for spectroscopic observations. An external capacitor C_{ext} (500 pF) has been used to measure transferred charges. A 1:1,000 high-voltage probe (Tektronix P6015A, Beaverton, OR, USA) measures the voltage across the DBD tube, and the Rogowski-type Pearson current monitor (model 110, 0.1V/A–1%, 1 Hz to 20 MHz, 20-ns usable rise time; Palo Alto, CA, USA) measures the total current flowing through the DBD tube. The total current and applied voltage waveforms are visualized by means of a four-channel Tektronix DPO 4054 digital oscilloscope. A VUV monochromator (MC; McPherson Model 302, Chelmsford, MA, USA) with a photomultiplier tube (PMT; McPherson Model 658) has been mounted on the vacuum chamber for the spectroscopic analysis of the discharges.

Relevant equations from equivalent electrical model for discharge analysis

The discharge information for the internal DBD parameters in sinusoidal and pulse excitations is obtained using an equivalent electrical circuit model [11-13]. An analogous electrical circuit for the coaxial DBD tube is shown in Figure 3 to calculate the internal electrical quantities such as discharge gas voltage $V_g(t)$, dielectric barrier voltage $V_d(t)$ (it is a series combination of upper barrier voltage $V_{d1}(t)$ and lower barrier voltage $V_{d2}(t)$ as shown in the figure), memory charge V_{m0}, discharge current $I_{dis}(t)$, supplied powers $P_{sup}(t)$ and consumed power $P_{dis}(t)$. The equations used to derive these parameters are expressed below for sinusoidal and pulse excitations, respectively. Here, C_g, C_d and $I_{dbd}(t)$ are used to represent the gas capacitance, barrier capacitance and current through DBD, respectively:

For sinusoidal excitation

$$I_{dis}(t) = \left(1 + \frac{C_g}{Cd}\right) I_{dbd}(t) - C_g \frac{dV_a(t)}{dt}, \quad (1)$$

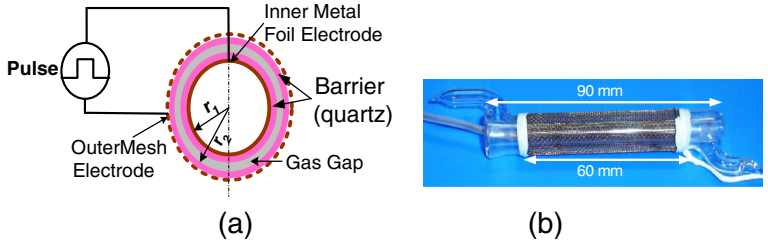

Figure 1 Schematic description of coaxial DBD tube (a) and fabricated xenon-filled coaxial DBD tube (b).

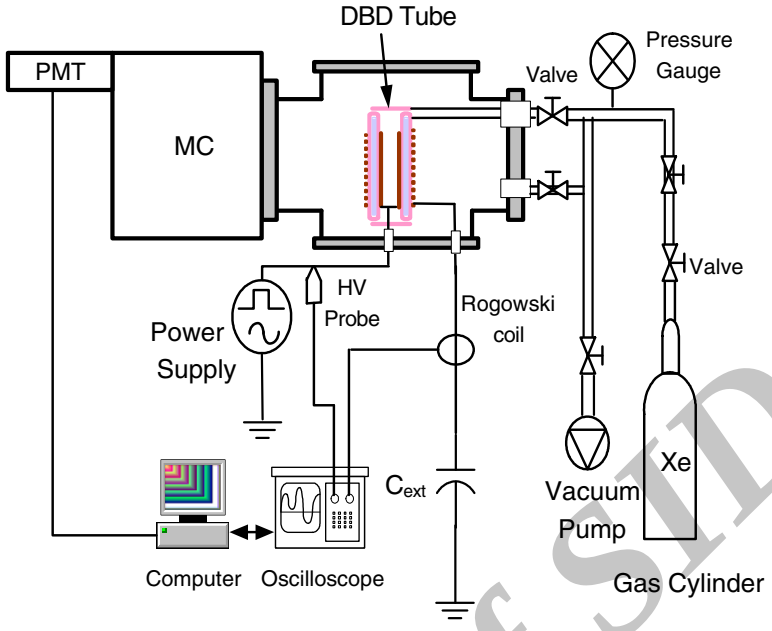

Figure 2 Schematic view of the experimental set-up.

$$V_d(t) = \frac{1}{C_d}\int I_{tc}(t)dt + V_{m0}, \tag{2}$$

$$V_g(t) = V_a(t) - \frac{1}{C_d}\int I_{tc}(t)dt - V_{m0}, \tag{3}$$

$$V_{m0} = -\frac{1}{2C_d}\int_0^{T/2} I_{dbd}(t)dt, \tag{4}$$

$$P_{\sup}(t) = V_a(t).I_{tc}(t), \tag{5}$$

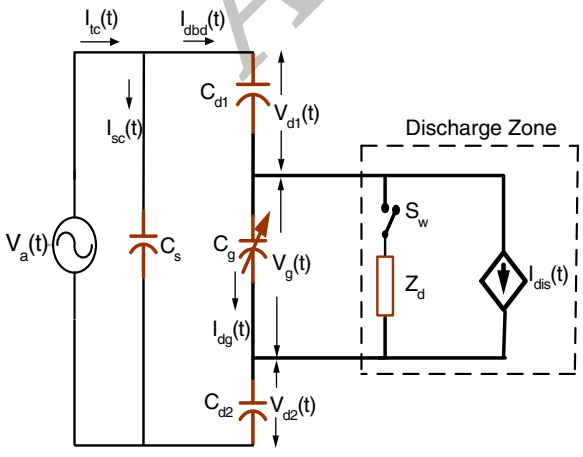

Figure 3 Equivalent electrical circuit model for coaxial DBD cell. (Adapted from [11]).

$$P_{dis}(t) = V_g(t).I_{dis}(t). \tag{6}$$

For pulse excitation

All the above equations are applicable except the discharge gas voltage $V_g(t)$, dielectric barrier voltage $V_d(t)$ and memory charge V_{m0}, which are given below:

$$V_d(t) = \frac{1}{C_d}\int I_{dbd}(t)dt = \frac{C_g}{C_g + C_d}V_a(t) + \frac{1}{C_g + C_d}\int_0^t I_{dis}(t)dt, \tag{7}$$

$$V_g(t) = V_a(t) - V_d(t) = \frac{C_d}{C_g + C_d}V_a(t) - \frac{1}{C_g + C_d}\int_0^t I_{dis}(t)dt, \tag{8}$$

$$V_m(t) = \frac{1}{C_g + C_d}\int_0^t I_{dis}(t)dt. \tag{9}$$

The gas capacitance C_g and barrier capacitance C_d are the input parameters used in the calculations that have been obtained from the geometry of the designed DBD source which are 15 and 26.63 pF, respectively.

Results and discussion

Discharge mode and electrical analysis

Figure 4a shows the average image of the discharge taken with a digital camera (SONY DSC-P100, Tokyo,

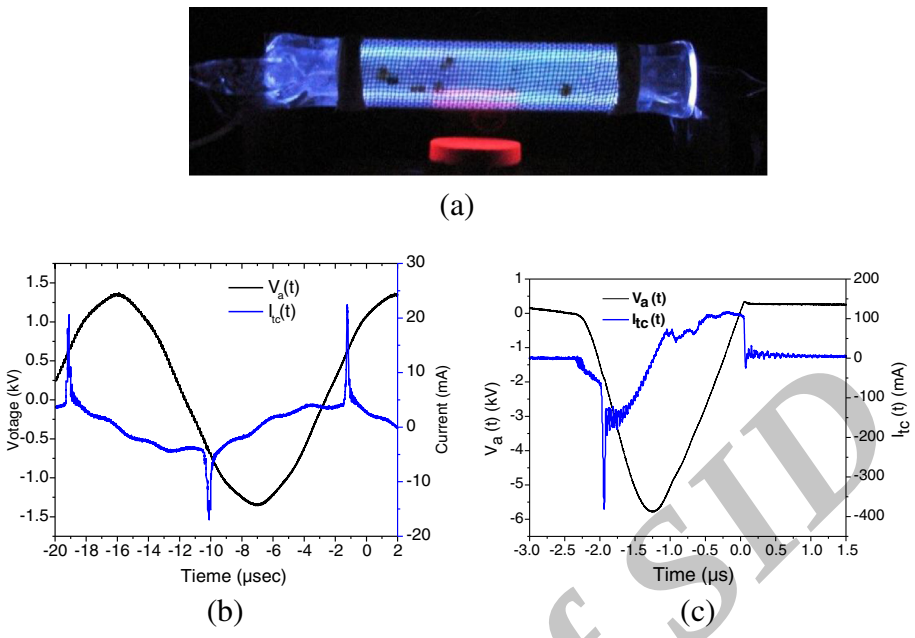

Figure 4 Diffused discharge in DBD cell and $V_a(t)$ and $I_{tc}(t)$ waveform in sinusoidal and pulse excitations. (**a**) Diffused discharge in xenon DBD cell (pressure 400 mbar, frequency = 30 kHz), (**b**) applied voltage $V_a(t)$ and total current $I_{tc}(t)$ waveforms in sinusoidal excitation (gas: xenon at 400 mbar, frequency = 55.5 kHz) and (**c**) applied voltage $V_a(t)$ and total current $I_{tc}(t)$ waveforms in pulse excitation (pressure 400 mbar, frequency = 30 kHz).

Japan; exposure time 25 ms) for the xenon coaxial DBD tube. The image indicates that the diffuse discharge covers the entire surface of the electrodes. Figure 4b,c shows the total current trace together with the applied voltages for sinusoidal and unipolar pulse excitations, respectively, where the discharge current waveform having only a few numbers of current pulses with a nanosecond order is superimposed on the total current.

In the experiment, the voltage applied to the metal foil electrode has been increased manually. When the applied voltage increased to a certain value, breakdown voltage V_{bd}, the discharge began with some filaments distributed on the dielectric wall, but the intensity of the visible light emitted from the discharge gap was very low. If the applied voltage is increased further, the number of filaments increases and finally gets diffused [14]. The discharge occurs at the rising front of the applied voltage waveform where the breakdown voltage is −1.78 kV in the case of pulse excitation and 0.6 kV in the case of sinusoidal excitation. In fact, the discharge current pulses include both the displacement current and the conduction current, which flow as soon as a conduction channel is formed when the gas breakdown takes place.

The dynamic behaviour of different voltages for the DBD tube for sinusoidal and pulse excitations is shown in Figure 5a,b. For this, the voltages across the dielectric, gas gap and memory voltage are calculated by Equations 2 to 4 and 7 to 9. The discharge occurs when the applied voltage reaches the breakdown voltage which results in significant electron production. After the breakdown, the produced electrons move towards the momentary anode driven by gap voltage and reverse the polarity of the initial memory voltage. The voltage across the dielectric, $V_d(t)$, starts increasing only when the discharge is initiated. Then, $V_d(t)$ rises rapidly for further increase of the discharge current. This rise is due to the charges from the plasma volume being collected on the surface of the dielectric. The gap voltage increases with the external applied voltage nearly at the same rate till the external voltage reaches the breakdown value. The small enhancement in the gap voltage marks the ignition condition. This corresponds to the weakening of the internal electric field in the gas gap due to momentary flow of the charges during discharge. It is observed that when breakdown occurs, the gas gap voltage and the external applied voltage are typically 0.4 and 0.6 kV, respectively, for the sinusoidal excitation while −1.5 and −1.8 kV, respectively, for the pulse excitation.

The instantaneous input power delivered by the electric supply $P_{sup}(t)$ and the power consumed during discharges $P_{dis}(t)$ are calculated by using Equations 5 and 6, respectively. Figure 5c,d shows the behaviour of the $P_{sup}(t)$ and $P_{dis}(t)$ for xenon DBD in sinusoidal and pulse excitations, respectively. During the rising front of the

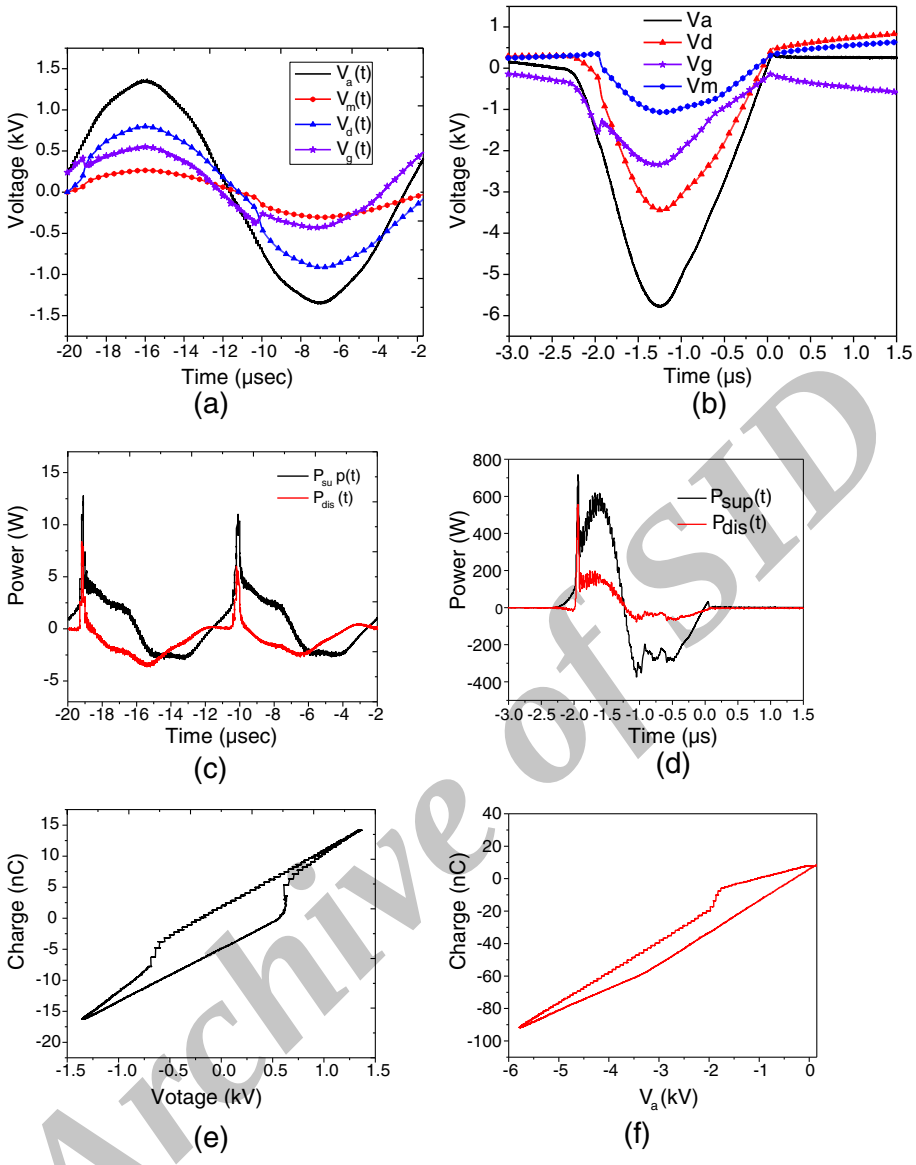

Figure 5 Experimental values of different voltages, supplied and discharge power, and Lissajous *V-Q* diagram of DBD. (**a**, **b**) Experimental values of different voltages for sinusoidal and pulse excitations, respectively; (**c**, **d**) Supplied and discharge power for sinusoidal and pulse excitations, respectively; (**e**, **f**) Lissajous *V-Q* diagram of the DBD for sinusoidal and pulse excitations, respectively. The sinusoidal voltage frequency is 55.5 kHz, while the unipolar pulse frequency is 30 kHz.

applied voltage, the $P_{sup}(t)$ includes both the power dissipated in the plasma and the reactive power stored in the various capacitors. The real power input occurs during the discharge phase. The characteristic of energy transfer to the DBD tube has been calculated by applying the Lissajous *V-Q* diagram, where the area enclosed within the *V-Q* curve is the energy deposited into the plasma per discharge cycle [15]. Figure 5e,f shows the Lissajous diagram for sinusoidal and pulse excitations, respectively. The total amount of power consumed by the DBD tube must be known in order to estimate both the total efficiency of the system and the required power of the HV supply. The energy consumed by the plasma for 1 cycle is calculated from the area of parallelograms for different operating conditions. It is found to be around 10 μJ for sinusoidal excitation while 61 μJ for pulse excitation.

Spectroscopic analysis

Figure 6a shows the occurrence of the first continuum at wavelength 151 nm and the second continuum at wavelength 172 nm in the DBD plasma source. The

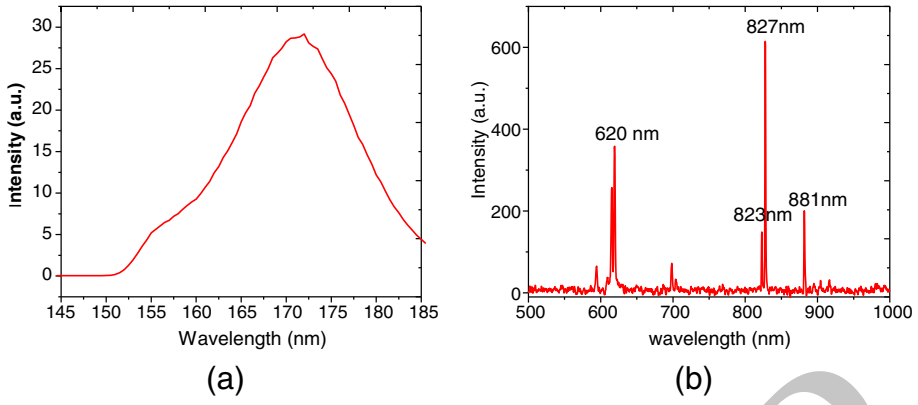

Figure 6 Spectra of xenon lamp in the (a) VUV region and (b) visible and near-infrared region.

vibrationally relaxed excimer molecules $Xe_2^*(0_u^+,\ v \approx 0)$ and $Xe_2^*(l_u,0_u^-,\ v \approx 0)$ decay subsequently through radiative processes by the following reactions and generate wavelength 172 nm in the DBD source [16]:

$$Xe_2{}^*(0_u{}^+, v{\approx}0){\rightarrow}Xe_2\left(0_g{}^+\right) + h\nu\left(\lambda_{peak} = 172\ \ nm\right), \tag{10}$$

$$Xe_2{}^*\left(1_u,0_u{}^-, v{\approx}0\right){\rightarrow}Xe_2\left(0_g{}^+\right) + h\nu\left(\lambda_{peak} = 172\ \ nm\right). \tag{11}$$

The similar mechanism happens for the continuum at wavelength 151 nm. This radiated wavelength is due to the molecular continuum with a peak at 151 nm and is referred as the first continuum of xenon excimer:

$$Xe_2{}^*(0_u{}^+, v >> 0){\rightarrow}Xe_2\left(0_g{}^+\right) + h\nu\left(\lambda_{peak} = 151\ \ nm\right) \tag{12}$$

$$Xe_2{}^*\left(1_u,0_u{}^-, v >> 0\right){\rightarrow}Xe_2\left(0_g{}^+\right) + h\nu\ \ \left(\lambda_{peak} = 151\ \ nm\right) \tag{13}$$

To illustrate it further, we can say that the electrons could have different energy distribution functions, which may lead to different electron kinetics and furthermore different occupations of excited states of xenon atom. In the next step of xenon excimer formation, different occupations of vibrational and electronic states of xenon excimer molecules could occur, which radiates the observed spectral lines. Besides these continuums in the xenon excimer radiation, the DBD source produces xenon atomic emission in the near-infrared region, i.e. 823 nm, 827 nm, etc. (see Figure 6b). These emission lines are due to radiative decay processes and atomic transitions from $Xe^{**}(6p)$ to $Xe^{*}(6s)$ [16]. To exploit the xenon atomic spectra for further analysis in the visible region, the radiated VUV light of specific wavelength 172 nm has been allowed to fall on red phosphor. The emission spectra of the xenon DBD tube using phosphor

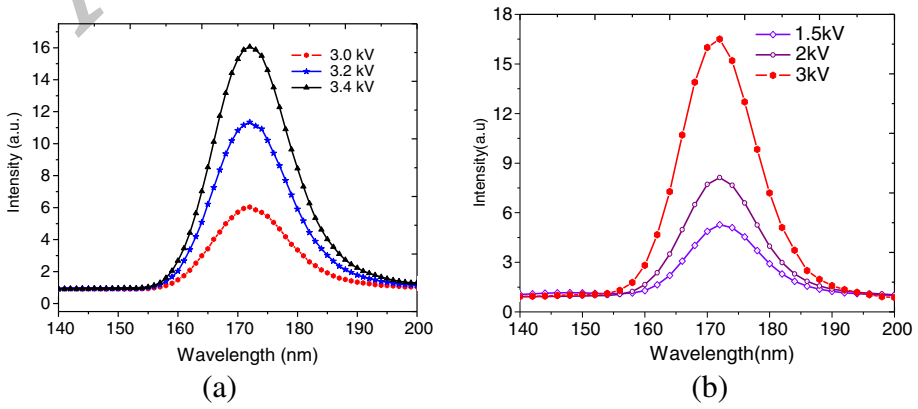

Figure 7 Comparison of relative intensity at 172 nm in different excitation methods. (**a**) Sinusoidal waveform, (**b**) unipolar pulse waveform (pressure 400 mbar, gap 1 mm, frequency 30 kHz).

is shown in Figure 6b. The spectral line 620 nm has been observed in the visible emission spectra that is due to the conversion of wavelength 172 nm and was not visible when red phosphor was absent. This observation can help in visible spectroscopic analysis. However, for direct analysis, a comparison of the radiated intensity of the spectral line 172 nm for sinusoidal and pulse excitations of the xenon DBD lamp has been made, as shown in Figure 7a,b, which helps in determining the effect of sinusoidal and pulse excitations on the performance of the DBD sources.

Figure 7a shows the relative intensity analysis of the Xe peak at wavelength 172 nm for sinusoidal excitation of radiations at different applied voltages and at a fixed frequency of 30 kHz, and it is observed that that the radiation power has increased with applied voltage. Similarly, the intensity due to pulse excitation increases with applied voltage as shown in Figure 7b at the same frequency. However, there is an interesting observation at 3 kV of applied voltage in the sinusoidal and pulse excitations of radiations. It has been observed that there is around three times increase in VUV intensity of the wavelength 172 nm at an applied voltage of 3 kV in the case of unipolar pulse excitation compared to that of sinusoidal excitation (see Figure 7a,b for comparison). The reduced field E/N of DBDs under unipolar pulse excitation varies dramatically in comparison to sine wave excitation [16-18] and perhaps is responsible for this effect. Furthermore, the enhanced performance of the pulsed DBD is derived from a discharge in the xenon DBD tube which is notably more uniform in spatial distribution of the discharge than that achieved using ac excitation [17]. The spatial uniformity keeps current densities and ionization rates low simultaneously compared with the filamentary operation and it is considered to be an important factor in respect of efficient electrical to radiative energy conversion in the plasma. Short pulses with fast rise time terminate discharge development right after ignition, thus significantly decreasing the ion heating power deposition in the vicinity of the electrodes. This effect results in an increase in discharge efficiencies.

Conclusions

The discharges useful for excimer light sources were examined in the Xe-filled coaxial DBD tube at different operating conditions. Visual images of the discharge and the electrical waveform confirm the diffused-type discharges. An electrical circuit model has been used for the discharge analysis of the DBD tube. The dynamic behaviour of the discharge parameters (barrier voltage, gas gap voltage, supplied power, consumed power, energy stored, etc.) and VUV radiation at 172 nm have been studied. The relative intensity analysis of the second Xe continuum peak in the VUV region shows around three times enhancement in the light radiation in pulse excitation compared to that in sinusoidal excitation which infers that the pulsed excitation of DBD sources is beneficial for excimer light sources.

Competing interests

The authors declare that they have no competing interests.

Authors' contributions

UNP carried out the basic study of DBD discharges, performed the statistical analysis and participated in the writing of the manuscript. PG participated in the design of the study and the analysis of the experimental data. NK participated in the design of the experimental set-up and experiments. MK participated in the design of the experimental set-up. VS participated in the design of the study. RP participated in the design of the study and drafted the manuscript. All authors read and approved the final manuscript.

Acknowledgements

The work has been carried out under CSIR Network Project (NWP0024). The authors are thankful to Mr. M. S. Tyagi and Mr. B. L. Meena for their useful help. Special thanks are also due to Dr. Chandra Shekhar and Dr. S. N. Joshi for their help, guidance and support.

Received: 30 October 2012 Accepted: 30 October 2012
Published: 28 November 2012

References

1. Becker, K.H., Kogelschatz, U., Schoenbach, K.H., Barker, R.J.: Non-Equilibrium Air Plasmas at Atmospheric Pressure. Institute of Physics, Beograd (2005)
2. Kogelschatz, U., Eliasson, B., Egli, W.: From ozone generators to flat television screens: history and future potential of dielectric-barrier discharges. Pure Appl. Chem. **71**, 1819 (1999)
3. Rehn, P., Wolkenhauer, A., Bente, M., Forster, R., Viol, W.: Wood surface modification in dielectric barrier discharges at atmospheric pressure. Surf. Coat. Technol. **174–175**, 515 (2003)
4. Kunhardt, E.E.: Generation of large-volume, atmospheric pressure, nonequilibrium plasmas. IEEE Trans. Plasma Sci. **2**(8), 189 (2000)
5. Radu, I., Bartnikas, R., Czeremuszkin, G., Wertheimer, M.: Diagnostics of dielectric barrier discharges in noble gases: atmospheric pressure glow and pseudoglow discharges and spatio-temporal patterns. IEEE Trans. Plasma Sci. **31**, 411 (2003)
6. Reece Roth, J., Rahel, J., Dai, X., Sherman, D.M.: The physics and phenomenology of One Atmosphere Uniform Glow Discharge Plasma (OAUGDP^{TM}) reactors for surface treatment applications. J. Phys. D: Appl. Phys. **38**, 555 (2005)
7. Rahel, J., Sherman, D.M.: The transition from a filamentary dielectric barrier discharge to a diffuse barrier discharge in air at atmospheric pressure. J. Phys. D: Appl. Phys. **38**, 547 (2005)
8. Liu, S., Neiger, M.: Excitation of dielectric barrier discharges by unipolar submicrosecond square pulses. J. Phys. D: Appl. Phys. **34**, 1632 (2001)
9. Liu, S., Neiger, M.: Double discharges in unipolar-pulsed dielectric barrier discharge xenon excimer lamps. J. Phys. D: Appl. Phys. **36**, 1565 (2003)
10. Valdivia-Barrientos, R., Pacheco-Sotelo, V., Pacheco-Pacheco, M., Benítez-Read, J.S., López-Callejas, R.: Analysis and electrical modeling of a cylindrical DBD configuration at different operating frequencies. Plasma Sources Sci. Technol. **15**, 237 (2006)
11. Pal, U.N., Sharma, A.K., Soni, J.S., Sonu, K., Khatun, H., Kumar, M., Meena, B.L., Tyagi, M.S., Lee, B.-J., Iberler, M., Jacoby, J., Frank, K.: Electrical modelling approach for discharge analysis of a coaxial DBD tube filled with argon. J. Phys. D: Appl. Phys. **42**, 045213 (2009)
12. Pal, U.N., Kumar, M., Tyagi, M.S., Meena, B.L., Khatun, H., Sharma, A.K.: Discharge analysis and electrical modeling for the development of efficient dielectric barrier discharge. J. Phys. Conf. Ser. **208**, 012142 (2010)
13. Udit Narayan, P., Pooja, G., Niraj, K., Mahesh, K., Tyagi, M.S., Meena, B.L., Sharma, A.K., Ram, P.: Analysis of discharge parameters in xenon-filled coaxial DBD tube. IEEE Trans. Plasma Sci. **39**(6), 1475 (2011)
14. Pal, U.N., Kumar, M., Khatun, H., Sharma, A.K.: Discharge characteristics of dielectric barrier discharge. J. Phys. Conf. Ser. **114**, 012065 (2008)
15. Takaki, K., Fujiwara, T.: Multipoint barrier discharge process for removal of NO_x from diesel engine exhaust. IEEE Trans. Plasma Sci. **29**(3), 518 (2001)

16. Lee, B.J.: Investigation of high-pressure microdischarges as sources of intense vacuum ultraviolet radiation. Ph.D. Thesis. University of Erlangen, (2007)
17. Mildren, R.P., Carman, R.J., Falconer, I.S.: Visible and VUV images of dielectric barrier discharges in Xe. J. Phys. D: Appl. Phys. **34**, 3378 (2001)
18. Beleznai, S., Mihajlik, G., Agod, A., Maros, I., Juhasz, R., Németh, Z., Jakab, L., Richter, P.: High-efficiency dielectric barrier Xe discharge lamp: theoretical and experimental investigations. J. Phys. D: Appl. Phys. **39**, 3777 (2006)

doi:10.1186/2251-7235-6-41
Cite this article as: Pal *et al.*: Analysis of discharge parameters and optimization study of coaxial DBDs for efficient excimer light sources. *Journal of Theoretical and Applied Physics* 2012 **6**:41.